Bifurcations of nonlinear localized modes in disordered lattices

Nikolaos K. Efremidis
Department of Applied Mathematics, University of Crete, Heraklion, 71409 Crete, Greece
(Received 10 April 2009; published 23 June 2009)

We analyze families of localized solutions of a nonlinear Schrödinger equation in the presence of a disordered potential modeling a waveguide array. A coupled mode theory approximation reveals that the families of disordered lattice solitons follow a cascade of Hopf-like bifurcations. Using a perturbation method, we analyze the origins of this bifurcation structure. We find that each family of solutions is characterized by a constant number of nodes. These predictions are in agreement with the numerical results of the nonlinear Schrödinger equation with a disordered potential.

DOI: 10.1103/PhysRevA.79.063831 PACS number(s): 42.65.Tg, 72.15.Rn, 42.25.Dd

I. INTRODUCTION

The phenomenon of localization in a disordered configuration has been studied for the first time in [1] and was motivated by experiments in spin waves. Anderson localization is a general wave phenomenon which applies in optical waves, sound waves, and quantum waves among others; however, the main application of this theory is related to the study of electrical transport phenomena in condensed-matter physics [2–5]. The dimensionality of the problem plays an important role in disordered settings. Using, a tight-binding model with a random potential, it is proved that in one spatial dimension all the linear modes are localized. In three dimensions, on the other hand, the modes in the center of the band are truly extended, whereas modes in the band edges are localized. In two dimensions it is believed that all the eigenstates are localized.

In addition, nonlinearity is a phenomenon that can also lead to the localization (or delocalization) of a wave packet. The study of this competition or synergy between nonlinearity and Anderson localization has attracted considerable attention especially during the last years. Theoretically, discrete breather formation in random lattices is studied in [6–8]. The diffusion of an initial wave packet in a random lattice is also investigated [9–13]. Experimentally, light propagation in disordered two-dimensional arrays of mutually coupled fibers is reported [14], while in [15] an experimental observation of Anderson localization in a perturbed periodic potential is observed. The linear and the nonlinear evolutions in an Anderson model of optical waveguides have been investigated in [16]. Several experiments have been performed in the context of Bose-Einstein condensates to study disorder, defects, and Anderson localization [17–21]. In these experiments the lattices can be quasiperiodic or laser speckles. Motivated by the recent experimental activity, in [22,23] a lattice Nonlinear Schrödinger (NLS) equation modeling disordered waveguide arrays in both one and two dimensions has been theoretically studied. In particular, families of disordered lattice solitons (DLSs) were analyzed and categorized to a few classes with the same qualitative properties.

In this paper, and in connection with our previous works [22,23], we analyze fundamental properties of lattice solitons in disordered lattices. We expand the solution in the linear localized modes (LLMs) of the lattice and apply a coupled mode theory (CMT) approximation. Analyzing the resulting system of equations, we find that there exists a cascade of Hopf-like bifurcations that the families of DLSs follow. As a result, by varying the eigenvalue (which is the bifurcation parameter), new families of solutions appear and the existing families exhibit significant changes in their profile due to spectral resonances. Families of DLSs can either have lower power thresholds or originate from the LLMs. In the case of two linear modes, asymptotic expressions for the solutions are derived. We find that for each family of solutions the number of nodes (or zeros) is conserved. We use a direct perturbation method to determine the nonlinear spectral changes related to the bifurcations of the solutions. Interestingly enough, in the related eigenvalue problems, only a few of the eigenvalues are shifted whereas most of the spectrum remains essentially invariant as compared to the linear case.

II. MODEL EQUATIONS

Let us consider the following NLS equation in one spatial dimension with a disordered potential:

$$i\frac{\partial \psi}{\partial z} + \frac{\partial^2 \psi}{\partial x^2} + V(x)\psi + \gamma|\psi|^2\psi = 0, \tag{1}$$

where ψ is the amplitude of the optical wave, x and z are the transverse and the propagation coordinates, and $\gamma=1$ ($\gamma=-1$) for self-focusing (self-defocusing) nonlinearity. The disordered potential $V(x)$ is proportional to the refractive index and the length of the array is x_0. In the case of zero boundary conditions the nonlinear modes of Eq. (1) close to the edge of the array are affected from the boundaries. On the other hand, in the case of periodic boundary conditions the modes close to the edge of the array see a disordered environment (exactly as the modes in the center of the array do). Thus, we prefer to solve Eq. (1) using periodic boundaries.

Different types of potentials $V(x)$ in Eq. (1) can describe different configurations or physical settings. In particular, optical waveguide arrays [16,24,25] can be modeled by step potentials where the amplitude is 0 or V_0. The spacing between successive waveguide centers L and the width of each waveguide W are uncorrelated random variables obeying

uniform distributions that take values in the ranges $2-0.4r \le L \le 2+0.4r$ and $1-0.4r \le W \le 1+0.4r$. We consider waveguides with average spacing $E[L]=2$ and average width $E[W]=1$. The parameter $0 \le r \le 1$ determines the degree of disorder of the array.

On the other hand, the index distribution $V(x)$ in optically induced lattices [15,26,27] is established by the interference of pairs of plane waves. Similar interference patterns can also be established in Bose-Einstein condensates [21]. We can model such configurations by setting $V=V_p+rV_d$, where

$$V_p(x) = \frac{V_0}{2}\cos\left(\frac{2\pi x}{L}\right) = \frac{V_0}{2}\cos\left(\frac{2\pi n_0 x}{x_0}\right) \tag{2}$$

is the periodic potential. V_0 is proportional to the maximum index or the potential contrast and the period of the potential is L. The potential V_p must satisfy the periodic boundaries, i.e., $x_0/L=n_0$ is an integer. The random potential is given by

$$V_d(x) = \frac{1}{V_m}\sum_{j=1}^{N} \alpha_j \cos\left(\frac{2\pi j x}{L} + \phi_j\right), \tag{3}$$

where α_j, ϕ_j are realizations of the uncorrelated random variables A, Φ, obeying uniform distributions with $-1 \le A \le 1$ and $0 \le \Phi \le 2\pi$. V_m is chosen such that $\max(|V_d|)=1$ while r is the degree of disorder.

Equation (1) has two integrals of motion, namely, the total power

$$P = \int_{-\infty}^{\infty} |\psi|^2 dx$$

and the Hamiltonian

$$H = \int_{-\infty}^{\infty} [|\psi_x|^2 + V(x)|\psi|^2 - (\gamma/2)|\psi|^4] dx.$$

Assuming stationary solutions of the form $\psi(x)=u(x)\times\exp(-iEz)$, we obtain

$$[E + V(x)]u + u_{xx} + \gamma u^3 = 0. \tag{4}$$

III. LINEAR PROPERTIES OF THE LATTICE

In the linear limit of Eq. (4) (i.e., $\gamma=0$) LLMs are solutions of the eigenvalue problem

$$[E + V(x)]u + u_{xx} = 0. \tag{5}$$

We enumerate the solutions (u_j, E_j) of Eq. (5) in increasing E order ($E_j < E_k$ if and only if $j<k$). From basic theorems in quantum mechanics, it is known that the number of nodes of a LLMs is an increasing function of E and, in particular, the jth LLM has exactly j zeros.

In Fig. 1(a) the first 120 eigenvalues forming a band structure are shown for a waveguide lattice of length $x_0=80$ with $r=1$ and $V_0=10$ having 42 waveguides. Through the rest of this paper, we are going to use this particular configuration unless stated otherwise. The shaded region in Fig. 1(a) separates the eigenvalues that originate from bound modes of each waveguide in isolation ($-10=-V_0 \le E \le 0$). In

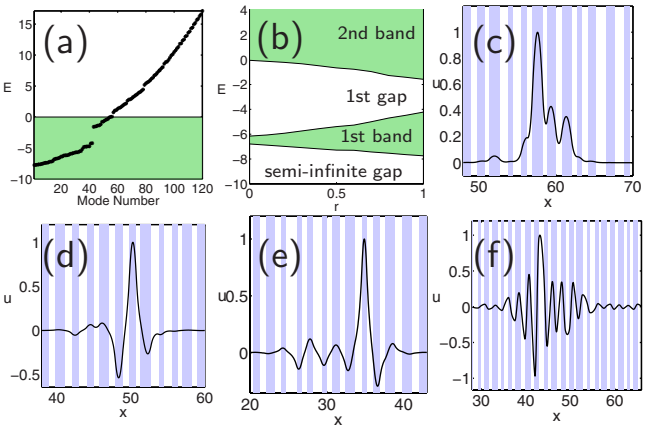

FIG. 1. (Color online) (a) Eigenvalues of the LLMs (enumerated in increasing E order) forming a band structure. (b) Regions of bands (shaded) and band gaps (white) as a function of the disorder parameter r. (c)–(f) LLMs 1, 23, 42, and 62, with eigenvalues $E=-7.74$, -6.17, -4.22, 1.55, respectively. Shaded regions in (c)–(f) represent high refractive index.

the case of a periodic lattice ($r=0$) the LLMs become periodic and extended Floquet-Bloch modes [28,29]. In a disordered lattice we define a band gap as a wide region between two successive eigenvalues of LLMs. In Fig. 1(a) we see that only one well-defined band gap opens up (between LLMs 42 and 43) separating the first band from the second semi-infinite band. As r increases the width of the bands increase and the surrounding gaps become smaller [Fig. 1(b)].

Let us point out that the LLMs of the NLS equation with a disordered potential exhibit several differences from those predicted by the corresponding discrete NLS. Such a discrete model is derived by applying CMT approximation in Eq. (1), i.e., $\psi(x,t)=e^{-iEt}\Sigma_{j=1}^{N} B_j(z)v_j(x)$, where $v_j(z)$ are the "local" modes of each waveguide in isolation (which are not orthogonal) and $B_j(z)$ are the complex amplitudes. The resulting discrete NLS equation takes the form

$$i\frac{dB_n}{dz} + \kappa_n B_{n-1} + \kappa_{n+1} B_{n+1} + \xi_n B_n + \gamma_1 |B_n|^2 B_n = 0, \tag{6}$$

where the parameters κ_n and ξ_n are random. The LLMs of CMT equations are strongly localized in the base and the edge of the band but are weekly localized in the middle of the band [2,3,16]. In addition, the localization length decreases symmetrically from the center to the edges of the first band. On the other hand, our results show that the localization length is a more complicated function of the parameters depending on the competition of two different mechanisms; according to which (i) the localization length decreases symmetrically with $E-E_c$ inside the first band (E_c is the center of the band) and (ii) the localization length increases as E increases. In the case of relatively small disorder and index modulations (for example, $r=0.3$, $V_0=10$ or $r=1$, $V_0=5$) the first mechanism is stronger inside the first band. On the contrary, in the case of strong disorder and large index contrasts (for example, $r=1$, $V_0=10, 20$; see Fig. 1) the second mechanism dominates. However, independently of the values of the parameters, for large enough E inside the second band,

the modes eventually become delocalized. Here, by the term "delocalized" we mean that the spatial extend of the mode is equal to the width of the lattice. Modes with eigenvalues in the region $-V_0<E<0$ [shaded region in Fig. 1(a)] are in general strongly localized [Figs. 1(c)–1(e)], whereas modes with $E>0$ are weekly localized [Fig. 1(f)] or delocalized. The delocalization of LLMs in the case of large enough E is observed for both zero and periodic boundary conditions. Notice that modes close to the base (edge) of the band are, in general, in phase (π out of phase) meaning that the phase difference among high-amplitude successive waveguides is zero or π.

IV. COUPLED MODE THEORY

A. Expansion in the linear localized modes

In the section, we expand the nonlinear wave in the LLMs of the lattice. Such an expansion is different from the one used in deriving Eq. (6) where the local modes of each waveguide in isolation were used. In particular, we assume that the evolution of a nonlinear optical wave can be asymptotically expressed as

$$\psi(x,t) = e^{-iEt}\sum_{j=1}^{N} A_j(z)u_j(x), \tag{7}$$

where $A_j(z)$ is the complex amplitude of the corresponding LLM and E is the propagation constant. Expansion (7) is valid as long as the nonlinear index change is smaller than the linear index contrast. Notice that we take into account the modes with the N lowest eigenvalues. For example, in the case of the lattice described in Sec. III, by setting $N=42$ we can include all the modes of the lowest band. Substituting Eq. (7) into Eq. (1) and using the orthogonality condition $(u_j,u_k)=\int u_j(x)u_k(x)dx=\delta_{j,k}$, we obtain

$$i\dot{A}_j + (E-E_j)A_j + \gamma\sum_{k,l,m=1}^{N}\sigma_{j,k,l,m}A_kA_lA_m^* = 0, \tag{8}$$

where

$$\sigma_{j,k,l,m} = \int_{-\infty}^{\infty} u_j(x)u_k(x)u_l(x)u_m(x)dx \tag{9}$$

is the overlap integral of the LLMs j, k, l, and m. In the case where one or more indices appear more than one time it might be more convenient to use the notation

$$\sigma_{j,k,l}^{a,b,c} = \int_{-\infty}^{\infty} u_j^a(x)u_k^b(x)u_l^c(x)dx, \tag{10}$$

where $a+b+c=4$ as well as

$$\sigma_j^4 = \int_{-\infty}^{\infty} u_j^4(x)dx, \quad \sigma_{j,k}^{a,b} = \int_{-\infty}^{\infty} u_j^a(x)u_k^b(x)dx, \tag{11}$$

where in the latter equation $a+b=4$. Notice that by definition the coefficients σ_j^4 and $\sigma_{j,k}^{2,2}$ are always positive. It might be interesting to point out that since the LLMs are orthogonal to each other, no linear coupling terms appear in Eqs. (8). Equations (8) involve summation over three different indices k, l, and m and thus this sum contains N^3 terms. Even the numerical solution of such systems is quite complicated. However, we can simplify this set of equations by taking into account the properties of the overlap integrals.

The overlap integral between the modes $u_j(x)$ and $u_k(x)$ is given by $\int u_j(x)u_k(x)dx$ and is smaller (or much smaller) than $\int u_j^2(x)dx=1$. Generalizing, in the case of overlap integrals between four different modes, we expect that the relations $\sigma_j^4 \gg |\sigma_{j,k}^{a_1,b_1}| \gg |\sigma_{j,k,l}^{a_2,b_2,c_2}| \gg |\sigma_{i,j,k,l}^{1,1,1,1}|$ hold (where j,k,l,m are constants and a_j,b_j are positive variables that satisfy the conditions $a_1+b_1=4$ and $a_2+b_2+c_2=4$). We found that the above relations are satisfied in our calculations using the numerically found LLMs of the disordered NLS equation. We utilize these inequalities by keeping terms with overlap integrals between at most two different LLMs

$$\begin{aligned} i\dot{A}_j + (E-E_j)A_j + \gamma\sigma_j^4|A_j|^2A_j + \gamma\sum_{\substack{k=1\\k\neq j}}^{N}\sigma_{j,k}^{1,3}|A_k|^2A_k \\ + \gamma\sum_{\substack{k=1\\k\neq j}}^{N}\sigma_{j,k}^{3,1}(2|A_j|^2A_k + A_j^2A_k^*) \\ + \gamma\sum_{\substack{k=1\\k\neq j}}^{N}\sigma_{j,k}^{2,2}(2|A_k|^2A_j + A_k^2A_j^*) = 0. \end{aligned} \tag{12}$$

The number of terms in each one of Eqs. (12) is now proportional to N.

B. Two-mode approximation

At this point we make the assumption that fundamental properties of DLSs can be found by analyzing the coupled mode equations (12) in the case of two linear modes ($N=2$). Such a simplified system is much easier to analyze both asymptotically and numerically. In particular, we are going to study the bifurcations of the solutions and in addition we are going to find asymptotic forms of the solutions. Our goal is to generalize these results for $N>2$. In the case $N=2$ Eqs. (12) become

$$\begin{aligned} i\dot{A}_1 + (E-E_1)A_1 + \gamma\sigma_1^4|A_1|^2A_1 + \gamma\sigma_{1,2}^{1,3}|A_2|^2A_2 \\ + \gamma\sigma_{1,2}^{3,1}(2|A_1|^2A_2 + A_1^2A_2^*) + \gamma\sigma_{1,2}^{2,2}(2|A_2|^2A_1 + A_2^2A_1^*) = 0, \end{aligned} \tag{13}$$

$$\begin{aligned} i\dot{A}_2 + (E-E_2)A_2 + \gamma\sigma_2^4|A_2|^2A_2 + \gamma\sigma_{1,2}^{3,1}|A_1|^2A_1 \\ + \gamma\sigma_{1,2}^{1,3}(2|A_2|^2A_1 + A_2^2A_1^*) + \gamma\sigma_{1,2}^{2,2}(2|A_1|^2A_2 + A_1^2A_2^*) = 0. \end{aligned} \tag{14}$$

Without loss of generality we can assume that $E_1<E_2$. Stationary solutions of Eqs. (12) can be obtained for real and constant amplitudes A_1,A_2, i.e.,

$$\begin{aligned} (E-E_1)A_1 + \gamma\sigma_1^4A_1^3 + \gamma\sigma_{1,2}^{1,3}A_2^3 \\ + 3\gamma\sigma_{1,2}^{3,1}A_1^2A_2 + 3\gamma\sigma_{1,2}^{2,2}A_2^2A_1 = 0, \end{aligned} \tag{15}$$

$$(E-E_2)A_2+\gamma\sigma_2^4A_2^3+\gamma\sigma_{1,2}^{3,1}A_1^3 + 3\gamma\sigma_{1,2}^{1,3}A_2^2A_1+3\gamma\sigma_{1,2}^{2,2}A_1^2A_2=0. \quad (16)$$

C. Asymptotic solutions

Different types of solutions for the algebraic set of Eqs. (15) and (16) can be asymptotically derived. These solutions are characterized according to their amplitudes (A_1,A_2). In particular, the amplitude of A_j can be large (positive $\longrightarrow$, negative $\longleftarrow$, or either of the signs $\longleftrightarrow$), small (positive $\rightarrow$, negative $\leftarrow$, or either of the signs $\leftrightarrow$), or very small $(\cdot)$. If (A_1,A_2) is a solution, $-(A_1,A_2)$ is also a solution. We can use this symmetry to set the amplitude of either A_1 or A_2 to be positive.

1. Solutions of the form $(\longrightarrow,\leftrightarrow)$

Solutions of the form $(\longrightarrow,\leftrightarrow)$ satisfy the condition

$$|A_2/A_1|\ll 1 \quad (17)$$

and in addition $A_1>0$. Eliminating small terms involving A_2 in Eq. (15) we find that

$$A_1\simeq\left(\frac{E_1-E}{\gamma\sigma_1^4}\right)^{1/2}. \quad (18)$$

A necessary condition for real solutions to exist is given by

$$\gamma(E_1-E)>0. \quad (19)$$

Thus, in the case of self-focusing nonlinearity $(\gamma=1)$ such solutions can exist for $E<E_1$, whereas if $\gamma=-1$ the eigenvalue should satisfy $E>E_1$. Substituting Eq. (18) into Eq. (16) under assumption (17) we find that A_2 is given by

$$A_2\simeq\frac{-\gamma\sigma_{1,2}^{3,1}A_1^3}{(E-E_2)+3\gamma\sigma_{1,2}^{2,2}A_1^2} =\frac{-\gamma\sigma_{1,2}^{3,1}}{E_1-E_2-\left(1-\frac{3\sigma_{1,2}^{2,2}}{\sigma_1^4}\right)(E_1-E)}\left(\frac{E_1-E}{\gamma\sigma_1^4}\right)^{3/2}. \quad (20)$$

Using Eqs. (18) and (20) the amplitude requirement (17) becomes

$$\left|\frac{A_2}{A_1}\right|\simeq\frac{\left|\frac{\sigma_{1,2}^{3,1}}{\sigma_1^4}(E_1-E)\right|}{\left|E_1-E_2-\left(1-\frac{3\sigma_{1,2}^{2,2}}{\sigma_1^4}\right)(E_1-E)\right|}\ll 1. \quad (21)$$

Inequality (21) is not satisfied when $E\simeq E_2$ in which case the denominator is close to zero. The interference of the two modes can be in phase or π out of phase and in particular $\mathrm{sgn}(A_2)=\mathrm{sgn}[\gamma\sigma_{1,2}^{3,1}(E_2-E)]$. For self-focusing nonlinearity $(E<E_1)$ the superposition of the two linear modes is in phase if $\sigma_{1,2}^{3,1}>0$ and out of phase if $\sigma_{1,2}^{3,1}<0$. On the other hand, in the self-defocusing case $(E>E_1)$ such solutions exist when the eigenvalue is far enough from the resonance $E=E_2$, i.e., $E_1<E\lesssim E_2$ and $E\gtrsim E_2$. In these two cases the sign of the superposition is opposite. For example, if $\sigma_{1,2}^{3,1}>0$ the amplitudes are in phase for $E_1<E\lesssim E_2$ and π out of phase for $E\gtrsim E_2$.

2. Solutions of the form $(\leftrightarrow,\longrightarrow)$

Solutions of the form $(\leftrightarrow,\longrightarrow)$ have similarities as compared to the solutions presented in the previous paragraph. In particular, the condition

$$|A_1/A_2|\ll 1 \quad (22)$$

should be satisfied and without loss of generality we assume that $A_2>0$. Since A_1 is small, Eq. (16) can be approximated by

$$A_2\simeq\left(\frac{E_2-E}{\gamma\sigma_2^4}\right)^{1/2}. \quad (23)$$

The necessary condition

$$\gamma(E_2-E)>0 \quad (24)$$

is obtained by requiring that the amplitude A_2 is real. Equation (24) is satisfied when $E<E_2$ $(E>E_2)$ in the case of self-focusing (self-defocusing) nonlinearity. Substituting Eq. (23) into Eq. (15) under assumption (22) we find that

$$A_1\simeq\frac{-\gamma\sigma_{1,2}^{1,3}A_2^3}{(E-E_1)+3\gamma\sigma_{1,2}^{2,2}A_2^2} =\frac{-\gamma\sigma_{1,2}^{1,3}}{(E_2-E_1)-\left(1-\frac{3\sigma_{1,2}^{2,2}}{\sigma_2^4}\right)(E_2-E)}\left(\frac{E_2-E}{\gamma\sigma_2^4}\right)^{3/2}. \quad (25)$$

Using Eqs. (23) and (25) the amplitude requirement given by Eq. (22) becomes

$$\frac{A_1}{A_2}\simeq\frac{-\frac{\sigma_{1,2}^{1,3}}{\sigma_2^4}(E_2-E)}{(E_2-E_1)-\left(1-\frac{3\sigma_{1,2}^{2,2}}{\sigma_2^4}\right)(E_2-E)}. \quad (26)$$

Notice that Eq. (26) is not satisfied for $E\simeq E_1$ in which case the denominator is close to zero. The sign of A_1 can be positive or negative depending on $\mathrm{sgn}(A_1)=\mathrm{sgn}[\gamma\sigma_{1,2}^{1,3}(E_1-E)]$. In the self-defocusing case $(E>E_2)$ Eq. (26) is always satisfied and in addition $\mathrm{sgn}(A_1)=\mathrm{sgn}(\sigma_{1,2}^{1,3})$. On the other hand, in the self-focusing case where $E<E_2$ such solutions exist far enough from the resonance $E=E_1$, i.e., for $E_1\lesssim E<E_2$ and $E\lesssim E_1$. The sign of the superposition is opposite in these two regions. For example, assuming that $\sigma_{1,2}^{1,3}>0$ the superposition is π out of phase for $E_1\lesssim E<E_2$ and in phase for $E\lesssim E_1$.

3. Solutions of the form $(\longrightarrow,\longleftrightarrow)$

The main property of solutions with amplitude profile $(\longrightarrow,\longleftrightarrow)$ is that both A_1 and A_2 are large and of the same order of magnitude. We restrict to the case $A_1>0$ and thus the two modes are in phase if $A_2>0$ or π out of phase if $A_2<0$. Since the condition $\sigma_j^4\gg|\sigma_{j,k}^{l,m}|$ is satisfied, Eqs. (15) and (16) are in first order decoupled; thus,

$$A_1\simeq\left(\frac{E_1-E}{\gamma\sigma_1^4}\right)^{1/2},\quad A_2\simeq\pm\left(\frac{E_2-E}{\gamma\sigma_2^4}\right)^{1/2}. \quad (27)$$

From Eqs. (27) the requirement that the amplitudes $|A_j|$ are large results to

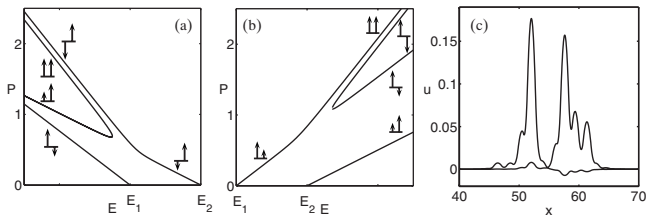

FIG. 2. Bifurcation diagrams depicting the power vs the propagation constant as obtained using CMT equations for (a) self-focusing and (b) self-defocusing nonlinearities. (c) The first two linear modes of the disordered lattice with overlap integrals $\sigma_1^4=0.0142$, $\sigma_{1,2}^{3,1}=-0.000\,646$, $\sigma_{1,2}^{2,2}=7.44\times10^{-5}$, $\sigma_{1,2}^{1,3}=0.000\,979$, and $\sigma_2^4=0.0215$ and eigenvalues $E_1=-7.744\,205$ and $E_2=-7.733\,342$.

$$(E_j-E)\gamma \gg \sigma_j^4, \quad j=1,2. \tag{28}$$

Typically $\sigma_j^4 \ll 1$ (see, for example, the parameters of Fig. 2 caption) and, thus, if $\gamma=1$ the eigenvalue range is $E \lesssim E_1$, whereas if $\gamma=-1$ we find that $E \gtrsim E_2$. In contrast to the families of solutions analyzed in the two previous paragraphs, for the same values of γ and E both the in-phase and π-out-of-phase solutions can exist.

D. Two-mode bifurcations

The bifurcations of DLSs in the case of two linear modes are studied here in the context of the CMT approximation. The algebraic set of Eqs. (15) and (16) are solved numerically using as initial conditions the approximate expressions derived in Sec. IV C. The first two LLMs of the disordered lattice shown in Fig. 1(c) are used to evaluate the σ coefficients of Eqs. (13) and (14).

In Figs. 2(a) and 2(b) the bifurcation curves depicting the total power $P=|A_1|^2+|A_2|^2$ vs the propagation constant E for $\gamma=\pm 1$ are shown. Notice that we use the term "total power" for convenience. In particular P equals to the sum of the squared amplitudes which equals to the total power if the LLMs have small overlaps. However, in the case of large overlaps between the LLMs there might be a significant deviation between P and the total power. We would like to point out that Eqs. (13) and (14) have a similar structure as compared to dynamical systems that exhibit Hopf bifurcations [30].

In Fig. 2(a) the self-focusing case is depicted. We see three different curves. One curve takes the form of the first linear mode $(\rightarrow,\cdot)$ close to the bifurcation point with the zero solution $(E=E_1)$. Since $\sigma_{1,2}^{3,1}<0$ the resulting nonlinear mode is π out of phase $(\longrightarrow,\leftarrow)$. The second family of solutions bifurcates from the second linear mode $(\cdot,\rightarrow)$ at $E=E_2$. The coefficient $\sigma_{1,2}^{1,3}$ is positive and thus the resulting wave $(\leftarrow,\longrightarrow)$ is π out of phase for $E_1 \lesssim E<E_2$. As it can be seen in Fig. 2(a) this family of solutions undergoes a bifurcation close to the resonant eigenvalue E_1 and for higher powers takes the form $(\longleftarrow,\longrightarrow)$. The sudden change in the slope of the existence curve close to $E=E_1$ is a consequence of the change in the form of the solution. The third family
of solutions shown in Fig. 2(a) is of purely nonlinear origin meaning that it exhibits a lower power threshold. The solutions in the lower branch of this family have the form $(\rightarrow,\longrightarrow)$. As expected these solutions exist in the region $E \lesssim E_1$ and are in phase since $\sigma_{1,2}^{1,3}>0$. The bifurcation structure for self-defocusing nonlinearity [Fig. 2(b)] is similar to the self-focusing case.

In the CMT equations, we define a node as a π phase difference in the amplitude of two successive LLMs, i.e., $A_jA_{j-1}<0$. The number of nodes remains constant (is conserved) for every family of solutions. There is a direct relationship between the number of nodes of the families of solutions with a power threshold and the number of nodes of particular families that originate from a linear mode. For example, in the self-focusing case shown in Fig. 2(a), if the family of solutions originating from LLM 2 has 0 (or 1) node then the nonlinear family of solutions will have 1 (or 0) node, respectively. As we will later see, the number of nodes is also conserved in the NLS equation with a disordered potential. However, there is no direct relation between the number of nodes of the CMT solutions and the nodes of the corresponding DLSs in the lattice NLS system. Finally, we would like to point out that in the high-intensity limit, four different branches of solutions exist for the same value of the propagation constant [for example, for $E \lesssim E_1$ in Fig. 2(a)].

E. General bifurcations

Applying the CMT approximation in the case of two linear modes we found that the families of solutions exhibit a Hopf-like bifurcation structure. However, the system has infinity of modes and even in a single-band approximation the number of modes is equal to the number of waveguides of the lattice. We would like to find if the bifurcation structure of the previous section is global in the sense that it is a fundamental pattern or building block that repeats itself (a cascade bifurcation). The simplest system that we are going to study to answer this question is a disordered lattice consisting of three linear modes.

We numerically solved Eqs. (8) in the case of three LLMs. However, the bifurcation diagram obtained are not clear enough because (i) bifurcation curves are very close to each other (and cannot be distinguished) and (ii) several curves cross each other. Instead of showing the exact bifurcation structure, we present a schematic illustration [Fig. 3] that is not realistic but is clear. In this figure the curves do not cross and are well separated from each other. All the other features of the CMT bifurcation structure are maintained.

In Fig. 3 we see that three families of solutions (a, b, and c) bifurcate from the linear modes, whereas five families have a lower power threshold. The number of nodes of these families of solutions is determined by specific σ coefficients of the system. However, in Fig. 3 we assume that families a, b, and c have 0, 1, and 2 nodes, respectively. The bifurcation structure of families a, b, and d was analyzed in the previous section. The additional families of solutions are related to the presence of the third mode (A). In particular, family of solutions c originates from the third linear mode (A). As the intensity increases the solutions takes the form of mode B until E approaches the resonant eigenvalue E_2. Close to this

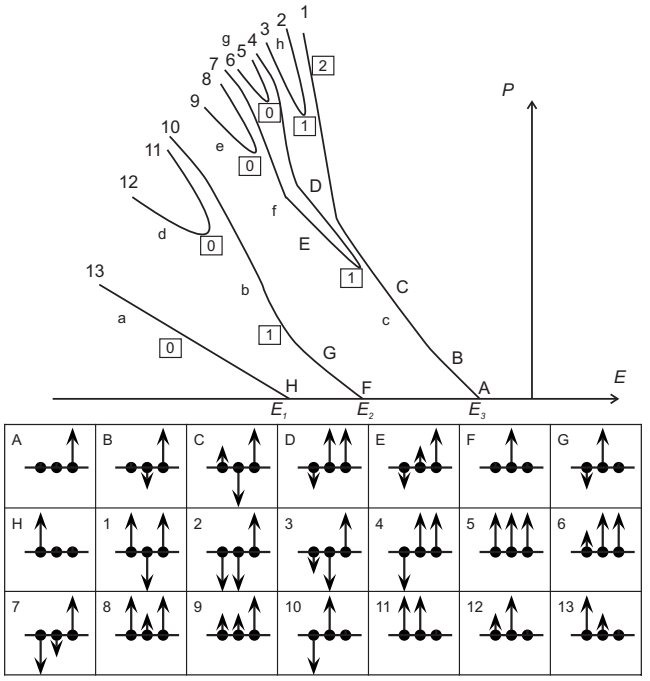

FIG. 3. Schematic illustration of the bifurcation curves (power P vs propagation constant E) in a disordered lattice with three LLMs for self-focusing nonlinearity. The amplitude profiles are shown in the bottom (A–H and 1–13). Eight different families of solutions exist (a–h). In square boxes the number of nodes of each family of solutions is shown.

resonance a Hopf-like bifurcation takes place and an additional family of solutions (f) appears. These two families of solutions (c and f) have three different branches (C, D, and E). For E close to the resonant eigenvalue E_1 each one of these branches undergoes an additional bifurcation giving rise to new families of solutions (e, g, and h).

We can generalize these results in the case of a lattice with N LLMs. In particular, close to the resonant eigenvalues E_j each different branch of solutions exhibits a Hopf-like bifurcation giving rise to an additional family of solutions (having two different branches). For a system consisting of N linear modes, we can count all different branches of solutions after each resonance and count how many different solutions (or branches) exist in the subsequent band gap. We assume self-focusing nonlinearity and for convenience we arrange the eigenvalues in the opposite direction as compared to Fig. 3, i.e., $E_N < E_{N-1} < \ldots < E_2 < E_1$. We define by F_j the number of different branches of solutions that exist due to the bifurcations associated with the resonant eigenvalue E_j. As the eigenvalue decreases and due to bifurcations associated with the eigenvalue E_{j+1} three different branches originate from each different branch. Thus we get $3F_j$ branches on the left of E_{j+1}. An additional family with one branch bifurcates from the zero solution exactly at $E=E_{j+1}$, and thus

$$F_{j+1} = 3F_j + 1. \tag{29}$$

We also know that $F_1=1$. Following the relevant algebra, we conclude that, deep enough inside the semi-infinite band gap,

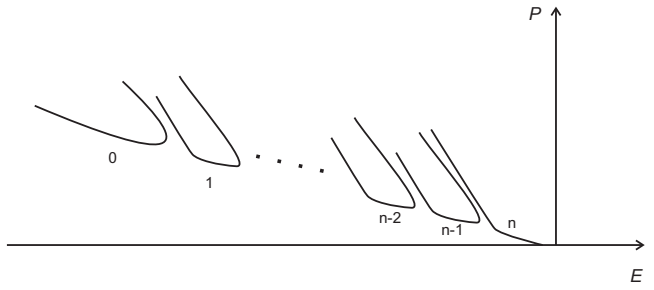

FIG. 4. Schematic illustration of the bifurcation structure of solutions in which the amplitude of one linear mode is much larger than the amplitudes of the remaining modes. The numbers in the figure indicate the nodes of the solution.

$$F_N = \sum_{j=0}^{N-1} 3^j = \frac{3^N - 1}{2}. \tag{30}$$

The discrete periodic case is described in Ref. [31]. Some of these solutions excite mainly one linear mode $(\leftrightarrow, \ldots, \leftrightarrow, \longrightarrow, \leftrightarrow, \ldots, \leftrightarrow)$, some excite a few of them (bound states), and the rest are extended solutions.

V. NODE CONSERVATION

We saw that in the case of CMT the number of nodes of a particular family of solutions is constant. Such a behavior is also encountered in the disordered NLS model. In particular if $u(x;E)$ is a family of solutions of Eq. (4) then the number of zeros $N(u(x,E))$ does not change with E (it is conserved). A nonrigorous proof is based on the fact that the solution $u(x;E)$ is a continuous function of x and E. We define the corresponding linear eigenvalue problem

$$L^- \phi_j^- = -\phi_{jxx}^- + V^-(x;E)E\phi_j^- = \lambda_j^-(E)\phi_j^-, \tag{31}$$

where $V^-(x;E) = -E - V(x) - \gamma u^2(x;E)$. The eigenvalues $\lambda_j^-(E)$ of the Sturm-Liouville problem with potential $V^-(x;E)$ are nondegenerate and also vary continuously with E. For a particular value of $E=E_0$ we can assume that $N(u(x;E_0)) = n-1$ and thus $u(x;E_0) = \phi_n^-(E_0)$. Since the eigenvalues $\lambda_j^-(E)$ do not "cross" we expect that $N(\phi_n^-(x;E)) = n-1$ for all values of E. Both functions $\phi_n^-(x;E)$ and $u(x;E)$ are continuous and coincide for $E=E_0$; thus, $\phi_n^-(x;E) = u(x;E)$.

Of particular interest are solitons that have single-hump profile. In the case of relatively strong disorder all (or most of) the linear modes with eigenvalues inside the first bands have such profile. By introducing nonlinearity such DLSs maintain a single-hump profile and the amplitude of a particular linear mode is much larger $(\rightarrow)$ than the amplitude of all the rest of the modes that can be small $(\leftrightarrow)$ or negligible $(\cdot)$. Solutions of this form can belong to different families because they have different numbers of zeros [see, for example, the solutions $(\rightarrow, \longrightarrow)$ and $(\leftarrow, \longrightarrow)$ in Fig. 2(a) or the solutions A, B, E, and 9 in Fig. 3].

In Fig. 4 a schematic illustration of the bifurcation structure of solutions having the general form $(\leftrightarrow, \ldots, \leftrightarrow, \longrightarrow, \leftrightarrow, \ldots, \leftrightarrow)$ is depicted. The family of DLSs that bifurcates from the zero solution at $E=E_{n+1}$ has the same number

of nodes as the corresponding LLM (i.e., n). Close to the resonance E_n a bifurcation takes place leading to a solution with a similar amplitude structure and $n-1$ nodes (the lower part of the $n-1$ curve). Each subsequent bifurcation taking place close to the resonances $E_{n-1}, E_{n-2}, \ldots$ reduces the number on nodes by one. Eventually, inside that gap the solution is in phase (has zero nodes).

VI. PERTURBATION METHOD

In Sec. IV using CMT we found that Hopf-like bifurcations take place close to the resonant eigenvalues $E \simeq E_j$ of the linear system. As we will see in the next section, this is also confirmed from our numerical calculations using the disordered NLS system. This might be surprising because the linear spectrum is expected to be altogether modified due to nonlinearity especially at high intensities [32]. It is also an indication that only a small part of the spectrum is significantly modified due to nonlinearity whereas the rest of the eigenvalues remain almost invariant.

Let

$$\psi_0 = u_0(x;E^0)\exp(-iE^0 t) \tag{32}$$

be a solution of Eq. (1), where the eigenvalue E^0 is constant and $u_0(x,E^0)$ is the amplitude that has m zeros $[N(u_0)=m]$. For simplicity in this section we assume that $\gamma=1$. We would like to find stationary solution for eigenvalues E close to E^0, that is, $E=E^0+\epsilon E^1$. We expand the solution as

$$\psi(x;E) = [u_0(x;E^0) + \epsilon u_1(x;E^0,E^1)]e^{-i(E^0+\epsilon E^1)t}. \tag{33}$$

and the first order is identically satisfied. Before proceeding any further, it is convenient to define the following eigenvalue problems:

$$L^{\pm}\phi_n^{\pm} = \lambda^{\pm}(E)\phi_n^{\pm}, \tag{34}$$

where the operators $L^{\pm}$ are given by

$$L^{\pm}(x;u,E)\phi_n^{\pm} = -\phi_{nxx}^{\pm} + V^{\pm}(x;u,E)\phi_n^{\pm}$$

and

$$V^{+}(x;u,E) = -E - V(x) - 3u(x;E)^2, \tag{35}$$

$$V^{-}(x;u,E) = -E - V(x) - u(x;E)^2. \tag{36}$$

For simplicity we denote $L^{\pm}=L^{\pm}(x;u_0,E^0)$ unless stated otherwise. The amplitude of the eigenfunctions $\phi_j^{\pm}$ can be normalized such that $(\phi_j^+,\phi_k^+)=\delta_{j,k}$ and $(\phi_j^-,\phi_k^-)=\delta_{j,k}$. Notice that $L^- u_0=0$, i.e., the operator L^- has $m-1$ negative eigenvalues and one zero eigenvalue $[u_0=\sigma_m(E)\phi_m^-, \lambda_m^-=0$, where $\sigma_m(E)$ is a normalization coefficient]. In addition $L^+ u_{0x} = V_x u_0$. The relation $V^+=V^--2u^2(x;E)$ results in a down shifting of the eigenvalue λ_j^+ as compared to λ_j^- $(\lambda_j^+<\lambda_j^-)$. Thus, at least all the first m eigenvalues λ_j^+ are going to be negative $(\lambda_j^+<0,\ j=1,\ldots,m)$. Our numerical calculations shown that solutions which are localized in the refractive index maxima have exactly m negative eigenvalues and the remaining eigenvalues are positive $(\lambda_j^+<0$ for $j\le m$ and $\lambda_j^+>0$ for $j>m)$.

In the next order $O(\epsilon)$ we get

$$L^+ u_1 = E^1 u_0. \tag{37}$$

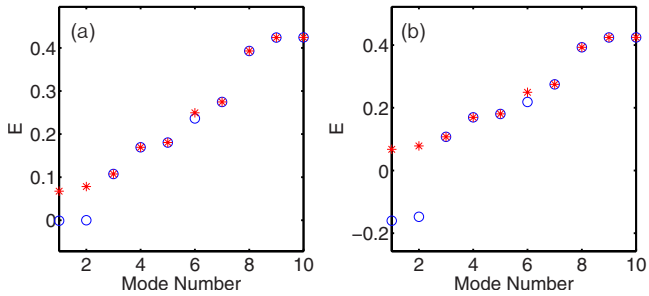

FIG. 5. (Color online) The lowest ten eigenvalues of the linear (stars) and nonlinear (circles) spectrum of the L^- (left) and the L^+ (right) operators. In particular, the nonlinear spectrum of a soliton family originating from the second linear mode is shown after the bifurcation with the first mode. Notice that the linear spectrum is shifted by E_2-E.

Thus, formally $u_1=E^1(L^+)^{-1}u_0$. The solution $u_1(x)$ can be expanded in the orthogonal set of eigenfunctions ϕ_j^+,

$$u_1(x) = \sum_j c_j \phi_j^+(x). \tag{38}$$

If we assume that the kernel of L^+ is null (which as we mentioned before is confirmed by our simulations) then the coefficients are given by

$$c_j = \frac{-E^1 \int_{-\infty}^{\infty} \phi_j^+(x)u_0(x)dx}{\lambda_j^+ \int_{-\infty}^{\infty} (\phi_j^+)^2 dx} = \frac{E^1}{\lambda_j^+}(\phi_j^+,u_0) \tag{39}$$

and the solution u_1 becomes

$$u_1(x) = E^1 \sum_j \frac{1}{\lambda_j^+}(\phi_j^+,u_0)\phi_j^+(x). \tag{40}$$

In Eq. (40) terms that have significant contribution are those with (i) large (ϕ_j^+,u_0) and (ii) small λ_j^+.

We numerically computed the evolution of the spectrum of the operators $L^{\pm}$ as the nonlinearity increases for DLSs originating from linear modes. In particular, in Fig. 5 the spectrum of a soliton family that bifurcates from the second linear mode is shown. In the linear limit the spectrum of the operators $L^{\pm}$ is identical with the spectrum of the linear problem (5). Thus, $\phi_j^-=\phi_j^+$ and only one term in Eq. (40) is nonzero and contributes in the perturbation

$$u_1(x) = \frac{E^1}{\lambda_m^+}(\phi_m^+,u_0)\phi_m^+(x) = \frac{E^1}{\lambda_m^+}u_0(x). \tag{41}$$

Equation (41) shows that for small intensities the spatial profile of the DLS is essentially the same with the spatial profile of the corresponding LLM and its amplitude increases as E^1 decreases $(\lambda_m^+<0)$. Due to nonlinearity, the eigenfunctions ϕ_j^+ become nonorthogonal with u_0 and, thus, all the terms in Eq. (40) have a nonzero contribution in the perturbation expansion. However, most of these terms remain very small and can be ignored. The nonlinear contribution in the potential V^+ is larger as compared to V^-. Thus, by increasing the

intensity the spectrum of L^+ is expected to be modified first. In particular, in the example of Fig. 5, the first significant change we observe in L^+ is a "flipping" of the two modes ϕ_1^+ and ϕ_2^+: the maximum amplitude of ϕ_1^+ (ϕ_2^+) changes position to the original location of the maximum amplitude of the ϕ_2^+ (ϕ_1^+). As a result the overlap integral (ϕ_1^+, u_0) becomes large in Eq. (40). After this flipping and for eigenvalues close to the resonance ($E \simeq E_1$) the magnitude of λ_2^+ decreases and becomes almost zero ($\lambda_2^+ \to 0^-$). Thus, both the coefficients of ϕ_1^+ and ϕ_2^+ are now large in Eq. (40). On the other hand, the spectrum of the remaining modes exhibit small changes as compared to the linear case and the respective overlap integrals in Eq. (40) remain small. We conclude that close to the resonance $E=E_1$ a good approximation is $u_1 \simeq E^1(c_1\phi_1^+ + c_2\phi_2^+)$, i.e., the amplitude of the solution is significantly modified in the locations of ϕ_j^+ ($j=1,2$). For even higher intensities the DLS eigenvalue lies inside the semi-infinite band gap $E<E_1$, and as it can be seen in Fig. 5, the two eigenvalues λ_1^- and λ_2^- are very close to each other $\lambda_2^- - \lambda_1^- \ll 1$. We would like to point out that besides $\lambda_{1,2}^{\pm}$ the remaining spectrum of the operators $L^{\pm}$ for does not exhibit significant changes even for relatively high intensities.

These results can be generalized in the case of a DLS that originates from linear mode m. In this case one by one after each bifurcation the first $m-1$ terms of Eq. (40) build up a large contribution in the expansion. On the other hand, the eigenvalues and the eigenfunctions of the modes with $j>m$ are not significantly modified as compared to the linear case.

VII. NUMERICAL SOLUTIONS

Families of DLSs supported by Eq. (1) are found by solving the corresponding stationary problem (4) using Newton's iteration scheme. In our previous works [22,23] we classified families of solutions according to their amplitude characteristics. Here, we analyze such families of solutions in connection with the results of the previous sections. In particular, we separately study families originating from LLMs and families with power thresholds.

A. DLSs originating from linear modes

A family of solutions that originates from a LLM (say E_j) does not have a power threshold. Clearly in the limit $E \to E_j$ the DLS power goes to zero $P \to 0$. However, for higher intensities, such DLSs can exhibit different properties according to the position of E_j inside the linear band structure.

For example in Fig. 3 we see three different families that originate from linear modes. These families bifurcate from the zero solution exactly at $E=E_j$ ($j=1,2,3$). In the case of m LLMs, one family of solutions bifurcates from each one of the linear modes. From these curves, only the family originating from E_1 does not exhibit bifurcations. The corresponding family of solutions in the disordered lattice studied here is shown in Fig. 6. As the peak intensity increases, the eigenvalue decreases and the DLS becomes narrower. For even higher peak intensities the induced nonlinear potential

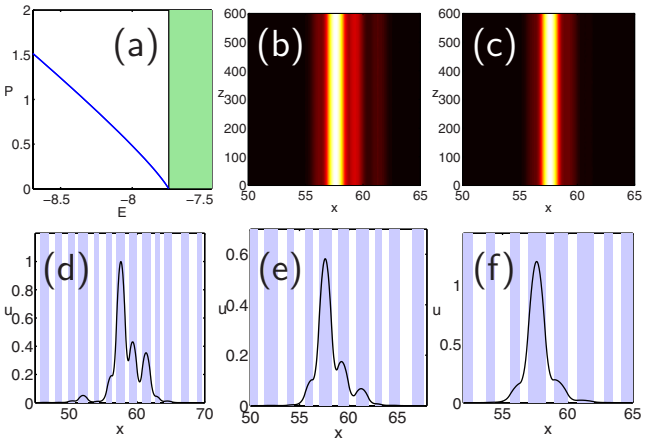

FIG. 6. (Color online) Self-focusing DLSs originating from the first LLM. (a) Power vs eigenvalue (bands are shown in shaded part); (d) LLM for $E=-7.74$; (b) and (c) stable propagation of the DLSs (e) and (f) with eigenvalues $E=-7.95, -8.69$, respectively.

becomes stronger than the random linear one, and the soliton takes the familiar hyperbolic secant profile.

The families of solutions that bifurcate from the zero solution at $E=E_m$ with $m>1$ exhibit Hopf-like bifurcations close to the resonant eigenvalues E_j ($j<m$) of the linear problem. These bifurcations do not happen exactly at $E=E_j$ because, due to nonlinearity, the spectrum is shifted. However, according to the analysis of Sec. VI the nonlinear shift of the relevant bifurcation eigenvalues is expected to be small.

In the example shown in Fig. 3 the family of solutions originating from E_3 exhibits bifurcations close to the resonant eigenvalues E_2 and E_1. We would like to point out that in the disordered NLS equation it can be a very difficult task to follow the exact bifurcation curve (such as the one described above) using Newton's iteration method, especially if the DLS and the LLM are spatially well separated. This happens because large spatial separation results in small values of the overlap integrals that involve these modes. As a consequence, subsequent bifurcation curves (such as the n and the $n-1$ curves shown in Fig. 4) come very close to each other. Thus, it is numerically possible to jump from one curve to another even with a very fine E step in Newton's scheme.

In Fig. 7, a family of solution originating from LLM 4 is shown. As the nonlinearity increases the DLS [Fig. 7(b)] has the tendency to become slightly more localized [Fig. 7(c)]. A bifurcation is expected to happen for $E \simeq E_3$. However the DLS and the third LLM with $E_3=-7.7$ have a large spatial separation. In our numerical results we were not able to follow this bifurcation. However, we did capture the subsequent bifurcation with the second LLM having $E_2=-7.733$ and maximum amplitude at $x \simeq 52$. In particular, as E approaches the eigenvalue of the linear mode, a bifurcation happens leading to a second peak in the soliton profile [Fig. 7(d) for $E \lesssim E_2$]. The resulting amplitude structure is a π-out-of-phase superposition of the two modes. Subsequently, the DLS bifurcates with the first LLM with $E_1 = -7.744$ and maximum amplitude at $x \simeq 56$ [Fig. 7(e) for

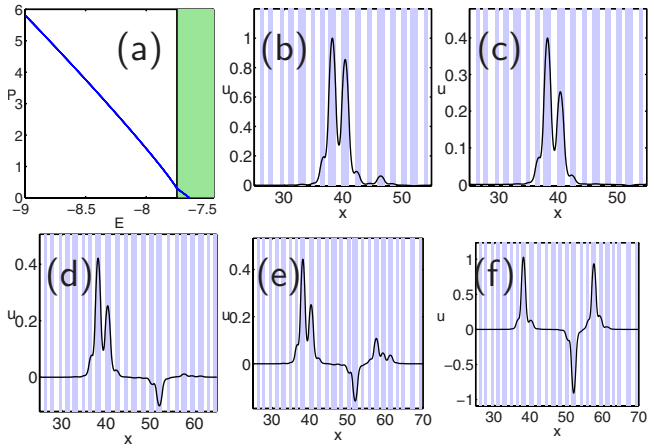

FIG. 7. (Color online) A Self-focusing family of DLSs originating from LLM 4. (a) P-E curve (bands are shown in shaded part); (b) LLM with $E=-7.64$; and (c)–(f) DLSs with $E=-7.73$, -7.74, -7.75, and -8.3, respectively.

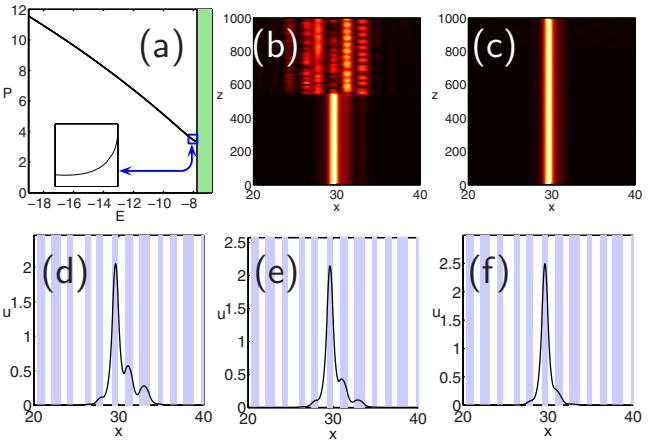

FIG. 8. (Color online) A family of self-focusing DLSs that exhibits lower amplitude and power thresholds localized on waveguide 16 of the lattice (a) P-E diagram; (d)–(f) DLSs with $E=-7.78,-8,-9$; and (b) and (c) depict dynamics of modes (e) and (f), respectively.

$E \lesssim E_1$]. Then, the eigenvalue enters the semi-infinite gap where no resonances are possible. As the nonlinearity further increases, the soliton has the tendency to become more localized close to the regions where the LLMs 4, 2, and 1 have maximum amplitude [Fig. 7(f)]. For even higher nonlinearity this DLS takes the form of three π-out-of-phase hyperbolic secants. Notice that all the modes shown in Fig. 7 are stable. Families of DLSs that bifurcate from the zero solution deep inside the band [say for $E=E_m$ $(m \gg 1)$] exhibit $m-1$ bifurcations leading to the eventual delocalization of the amplitude profile which can occupy the entire array.

B. DLSs exhibiting power thresholds

Using CMT (Fig. 3) we predicted that in the case of a system with three LLMs, five different families of solutions exhibiting power thresholds exist. Each family has two different branches (the "upper" and the "lower"). From these ten different branches, two represent single peak DLSs (9 and 12) and eight are bound states. An additional branch of single peak hump solution which does not exhibit lower power threshold is 13. In this section we numerically analyze single-hump DLSs supported by the disordered NLS equation that exhibit lower power thresholds.

Highly confined DLSs inside the gaps can be found using initial conditions that are strongly localized in a single waveguide. In the self-focusing case, the initial condition is asymptotically given by a hyperbolic secant and its eigenvalue lies in the semi-infinite gap. We find 42 different families of such solitons, each one of them centered in each of the 42 waveguides. All these families of DLSs have zero nodes. As expected, one of these families, which was analyzed in the previous section (see Fig. 6), does not exhibit power thresholds.

The remaining 41 families of DLSs are lower branches of families that exhibit lower power and amplitude thresholds, i.e., both $P(E)$ and $\|u(E)\|_\infty$ are bounded from below. A typical example is shown in Fig. 8. In particular we see that as the peak intensity decreases the DLS becomes broader. After some point, the slope in the P-E curve turns positive (an indication that there is an additional upper branch). This family of solutions exists for $E \lesssim -7.8$. Notice that DLSs belonging to this family are stable for strong nonlinearities, whereas for weaker nonlinearities the slope changes and they turn unstable [Figs. 8(b) and 8(c)].

In a similar fashion self-defocusing DLSs that are strongly localized in a single waveguide of the lattice can also exist in the finite gap of the spectrum. Again, the number of nodes of such solutions is equal to the number of waveguides of the lattice (42 in our case). In addition, these DLSs have a π phase difference between successive waveguides. A typical example of a DLS with lower amplitude and power thresholds is shown in Fig. 9. Notice that this family of solutions exists for eigenvalues $E \gtrsim -4$. Decreasing the eigenvalues the solution becomes broader up to $E \simeq -4$. On the other hand, by increasing the nonlinearity, the eigenvalue enters the second band where, due to successive bifurcations with the modes of the lattice, the DLS becomes delocalized and unstable [Fig. 9(c)].

VIII. CONCLUSIONS

We have studied in detail the properties of families of DLSs. We used three different approaches. The first is based on the CMT expansion of the wave in the LLM. In addition,

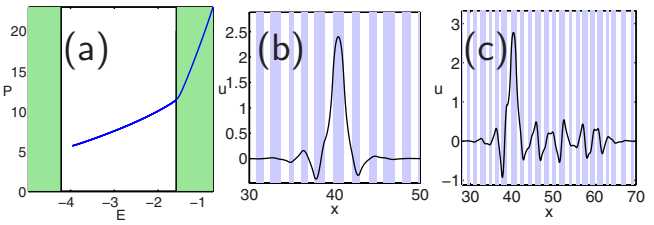

FIG. 9. (Color online) (a)–(c) A family of DLSs localized on waveguide 22 that exhibits lower amplitude and power thresholds; (a) P-E diagram and DLSs for (b) $E=-3$ and (c) $E=-1.4$.

we applied a perturbation method around the DLS solution. The last approach is the direct solution of the disordered NLS equation using Newton's iteration scheme. Using these methods, we analyzed the bifurcations of the solutions and the spectrum of the linearized operators. We found that families of DLSs exhibit a cascade of Hopf-like bifurcations. In addition, we showed that each family of solutions is characterized by a constant number of nodes.

[1] P. Anderson, Phys. Rev. **109**, 1492 (1958).
[2] P. A. Lee and T. V. Ramakrishnan, Rev. Mod. Phys. **57**, 287 (1985).
[3] D. Belitz and T. R. Kirkpatrick, Rev. Mod. Phys. **66**, 261 (1994).
[4] J. D. Maynard, Rev. Mod. Phys. **73**, 401 (2001).
[5] P. Sheng, *Introduction to Wave Scattering, Localization and Mesoscopic Phenomena* (Springer, Berlin, 2006).
[6] G. Kopidakis and S. Aubry, Phys. Rev. Lett. **84**, 3236 (2000).
[7] G. Kopidakis and S. Aubry, Physica D **130**, 155 (1999).
[8] G. Kopidakis and S. Aubry, Physica D **139**, 247 (2000).
[9] M. I. Molina, Phys. Rev. B **58**, 12547 (1998).
[10] A. Trombettoni, A. Smerzi, and A. R. Bishop, Phys. Rev. Lett. **88**, 173902 (2002).
[11] T. Kottos and M. Weiss, Phys. Rev. Lett. **93**, 190604 (2004).
[12] G. Kopidakis, S. Komineas, S. Flach, and S. Aubry, Phys. Rev. Lett. **100**, 084103 (2008).
[13] S. Flach, D. O. Krimer, and C. Skokos, Phys. Rev. Lett. **102**, 024101 (2009).
[14] T. Pertsch, U. Peschel, J. Kobelke, K. Schuster, H. Bartelt, S. Nolte, A. Tünnermann, and F. Lederer, Phys. Rev. Lett. **93**, 053901 (2004).
[15] T. Schwartz, G. Bartal, S. Fishman, and M. Segev, Nature (London) **446**, 52 (2007).
[16] Y. Lahini, A. Avidan, F. Pozzi, M. Sorel, R. Morandotti, D. N. Christodoulides, and Y. Silberberg, Phys. Rev. Lett. **100**, 013906 (2008).
[17] C. Fort, L. Fallani, V. Guarrera, J. E. Lye, M. Modugno, D. S. Wiersma, and M. Inguscio, Phys. Rev. Lett. **95**, 170410 (2005).
[18] L. Sanchez-Palencia, D. Clément, P. Lugan, P. Bouyer, G. V. Shlyapnikov, and A. Aspect, Phys. Rev. Lett. **98**, 210401 (2007).
[19] B. Shapiro, Phys. Rev. Lett. **99**, 060602 (2007).
[20] J. Billy, V. Josse, Z. Zuo, A. Bernard, B. Hambrecht, P. Lugan, D. Clement, L. Sanchez-Palencia, P. Bouyer, and A. Aspect, Nature (London) **453**, 891 (2008).
[21] G. Roati, C. D'Errico, L. Fallani, M. Fattori, C. Fort, M. Zaccanti, G. Modugno, M. Modugno, and M. Inguscio, Nature (London) **453**, 895 (2008).
[22] N. K. Efremidis and K. Hizanidis, Phys. Rev. Lett. **101**, 143903 (2008).
[23] N. K. Efremidis, Opt. Lett. **34**, 596 (2009).
[24] D. N. Christodoulides and R. I. Joseph, Opt. Lett. **13**, 794 (1988).
[25] H. S. Eisenberg, Y. Silberberg, R. Morandotti, A. R. Boyd, and J. S. Aitchison, Phys. Rev. Lett. **81**, 3383 (1998).
[26] N. K. Efremidis, S. Sears, D. N. Christodoulides, J. W. Fleischer, and M. Segev, Phys. Rev. E **66**, 046602 (2002).
[27] J. W. Fleischer, M. Segev, N. K. Efremidis, and D. N. Christodoulides, Nature (London) **422**, 147 (2003).
[28] P. J. Y. Louis, E. A. Ostrovskaya, C. M. Savage, and Y. S. Kivshar, Phys. Rev. A **67**, 013602 (2003).
[29] N. K. Efremidis and D. N. Christodoulides, Phys. Rev. A **67**, 063608 (2003).
[30] The stationary points of Eqs. (13) and (14) are given by Eqs. (15) and (16). This latter algebraic system has a similar structure as compared to a generalized stationary form of either the Hopf dynamical system or a coupled imperfect pitchfork system. The normal forms of the Hopf and the pitchfork models are $\dot{x}_1=\alpha x_1-x_2-x_1(x_1^2+x_2^2)$, $\dot{x}_2=x_1+\alpha x_2-x_1(x_1^2+x_2^2)$, and $\dot{x}=\alpha x-x^3$, respectively. Notice that the bifurcation structure shown in Fig. 2 is characteristic of an imperfect pitchfork bifurcation. Since Eqs. (13) and (14) are complex the stability of the solutions is different as compared to the corresponding real model. The term "Hopf-like" bifurcation is used here because the nonzero states are not stationary but oscillate during propagation.
[31] J. C. Eilbeck, P. S. Lomdahl, and A. C. Scott, Physica D **16**, 318 (1985).
[32] In disordered lattices the linear modes are spatially localized. Nonlinearity modifies the potential of the relevant linear eigenvalue problems ($L^{\pm}$) and thus *all* their eigenvalues. In contrast, localized changes in the potential of uniform and periodic systems modify the extended eigenfunctions of the continuous spectrum but the eigenvalues remain the same.